

## Mechanistically Guided Design of Ligands that Significantly Improve the Efficiency of CuH-Catalyzed Hydroamination Reactions

Andy A Thomas, Klaus Speck, Ilia Kevlishvili, Zhaohong Lu, Peng Liu, and Stephen L. Buchwald

*J. Am. Chem. Soc.*, **Just Accepted Manuscript** • DOI: 10.1021/jacs.8b09565 • Publication Date (Web): 23 Sep 2018

Downloaded from <http://pubs.acs.org> on September 23, 2018

### Just Accepted

“Just Accepted” manuscripts have been peer-reviewed and accepted for publication. They are posted online prior to technical editing, formatting for publication and author proofing. The American Chemical Society provides “Just Accepted” as a service to the research community to expedite the dissemination of scientific material as soon as possible after acceptance. “Just Accepted” manuscripts appear in full in PDF format accompanied by an HTML abstract. “Just Accepted” manuscripts have been fully peer reviewed, but should not be considered the official version of record. They are citable by the Digital Object Identifier (DOI®). “Just Accepted” is an optional service offered to authors. Therefore, the “Just Accepted” Web site may not include all articles that will be published in the journal. After a manuscript is technically edited and formatted, it will be removed from the “Just Accepted” Web site and published as an ASAP article. Note that technical editing may introduce minor changes to the manuscript text and/or graphics which could affect content, and all legal disclaimers and ethical guidelines that apply to the journal pertain. ACS cannot be held responsible for errors or consequences arising from the use of information contained in these “Just Accepted” manuscripts.

# Mechanistically Guided Design of Ligands that Significantly Improve the Efficiency of CuH-Catalyzed Hydroamination Reactions

Andy A. Thomas,<sup>†§</sup> Klaus Speck,<sup>†§</sup> Ilia Kevlishvili,<sup>†‡</sup> Zhaohong Lu,<sup>§</sup> Peng Liu,<sup>‡\*</sup> and Stephen L. Buchwald<sup>§\*</sup>

Submitted to the  
*Journal of the American Chemical Society*

Address Correspondence to:  
Professor Stephen L. Buchwald  
18-490 Dreyfus Laboratory  
Department of Chemistry  
Massachusetts Institute of Technology  
77 Massachusetts Avenue,  
Cambridge, MA 02139

tel: (617) 253-1885  
FAX: (617) 253-3297  
e-mail: slbuchwald@mit.edu

## ABSTRACT

Using a mechanically guided ligand design approach, a new ligand (SEGFASST) for the CuH-catalyzed hydroamination reaction of unactivated terminal olefins has been developed, providing a 62-fold rate increase over reactions compared to DTBM-SEGPBOS, the previous optimal ligand. Combining the respective strengths of computational chemistry and experimental kinetic measurements, we were able to quickly identify potential modifications that lead to more effective ligands, thus avoiding synthesizing and testing a large library of ligands. By optimizing the combination of attractive, non-covalent ligand-substrate interactions and the stability of the catalyst under the reaction conditions, we were able to identify a finely-tuned hybrid ligand that greatly enables accelerated hydrocupration rates with unactivated alkenes. Moreover, a modular and robust synthetic sequence was devised, which allowed for practical, gram-scale synthesis of these novel hybrid ligand structures.

## INTRODUCTION

In 2013, Buchwald,<sup>1</sup> and Miura and Hirano<sup>2</sup> independently demonstrated that copper hydride complexes (LCuH) can catalyze the chemo- and enantioselective hydroamination reactions between olefins and hydroxylamine esters (Figure 1a). Since then the generality and applicability of this approach has been well demonstrated for a variety of substrates such as styrenes,<sup>3</sup> vinylsilanes,<sup>4</sup> alkynes<sup>5</sup> and occasionally unactivated olefins,<sup>6</sup> highlighting its enormous potential. Despite these achievements hydroamination reactions catalyzed by LCuH are not without limitations.<sup>7</sup> For example, transformation of coupling partners such as cyclic, internal, and some unactivated terminal olefins often require elevated temperatures and increased reaction times compared to those of activated substrates.<sup>8</sup> In particular, an efficient *anti*-Markovnikov hydroamination reaction with unactivated terminal olefins is highly desirable, because the products of these reactions are frequently found in bioactive molecules.<sup>9</sup> These compounds are traditionally prepared by transforming carbonyl compounds, amides or alkyl electrophiles into their corresponding amine products.<sup>10</sup> From a strategic standpoint, hydroamination reactions between olefins and electrophilic amine sources provide one of the most straightforward and general avenues to access these important motifs, especially since the precursors are typically stable, readily available, and easy to handle.<sup>11</sup>

Recently, several experimental<sup>12,13</sup> and computational<sup>14</sup> mechanistic investigations have appeared on both CuH catalyzed hydroamination and hydroboration reactions, revealing the same basic catalytic cycle, comprised of four elementary steps: hydrocupration (I), oxidative addition (II), reductive elimination (III) and  $\sigma$ -bond metathesis (IV) (Figure 1b).<sup>15</sup> These studies demonstrated that the rate determining step (RDS) can vary between different olefinic substrates. Specifically, the RDS for activated substrates, such as styrenes, is often the catalyst regeneration

by  $\sigma$ -bond metathesis, whereas it changes to the hydrocupration step for unactivated internal or terminal alkenes,<sup>12,14</sup> indicating that the lower reactivity observed for unactivated olefins is the direct result of higher barriers for hydrocupration.

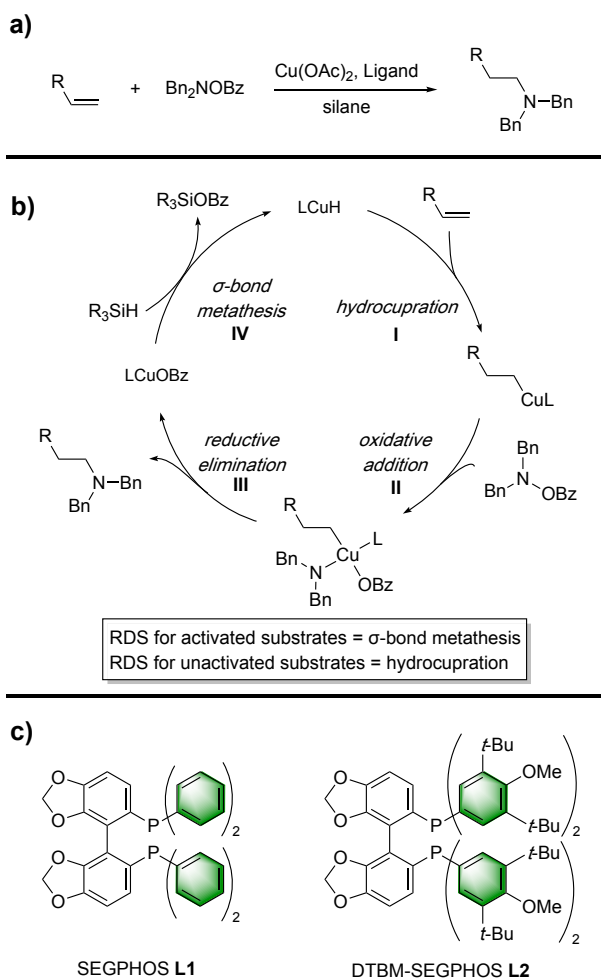


**Figure 1.** a) LCuH-catalyzed *anti*-Markovnikov hydroamination reaction. b) Proposed catalytic cycle for LCuH-catalyzed *anti*-Markovnikov hydroamination reaction. c) SEGPHOS L1 and DTBM-SEGPHOS L2 ligands.

Typically, reaction development in this area has relied on empirical observations pertaining to which catalytic system provides the fastest reaction rates.<sup>12</sup> For example, reactions with SEGPHOS L1 supported LCuH catalysts are often found to be slower; whereas, the use of

1  
2  
3 sterically more demanding DTBM-SEGPHOS **L2** derivative is often key to achieving higher  
4 reactivity, especially in the reactions of unactivated olefins (Figure 1c).<sup>12</sup>  
5  
6

7  
8 Beginning last year, our laboratories sought to unravel the theoretical foundations that  
9 lead to favorable hydrocupration events between LCuH (L = **L1** and **L2**) and various unactivated  
10 olefins, by performing the ligand-substrate interaction model analysis on this crucial step (Figure  
11 2a).<sup>14a</sup> Using this approach, the contributions of the different types of catalyst-substrate  
12 interactions to the overall activation energy ( $\Delta E^\ddagger$ ) were split into three categories: (1) the  
13 distortion energy required for the LCuH and the substrate to reach their transition state  
14 geometries ( $\Delta E_{\text{dist}}$ ); (2) the through-space interactions between the ligand and the substrate ( $\Delta E_{\text{int-}}$   
15  $\text{space}$ ); and (3) the through-bond interactions between the CuH moiety and the substrate ( $\Delta E_{\text{int-}}$   
16  $\text{bond}$ ). In the hydroamination reactions when SEGPHOS **L1** and DTBM-SEGPHOS **L2** ligands  
17 were employed, the  $\Delta E_{\text{dist}}$  and  $\Delta E_{\text{int-bond}}$  terms were not found to correlate with the overall  
18 activation energies ( $\Delta E^\ddagger$ ); however, excellent linear correlations were observed with  $\Delta E_{\text{int-space}}$ .  
19 This suggested that the *t*-butyl substituents at the 3- and 5-positions on the *P*-aryl<sub>2</sub> groups in  
20 DTBM-SEGPHOS **L2** promote stabilizing non-covalent interactions (Figure 2b). Indeed,  
21 dissecting the  $\Delta E_{\text{int-space}}$  term into its individual components revealed that attractive London  
22 dispersion forces ( $\Delta E_{\text{disp}}$ ) between the 3,5-di-*t*-butyl substituents on the *P*-aryl<sub>2</sub> groups and the  
23 substrate were the main contributing factor to achieve high catalyst activity with the DTBM-  
24 SEGPHOS **L2** ligand. While the London dispersion interactions are relatively weak (0.5~1.5  
25 kcal/mol for interactions with each *t*-Bu substituent),<sup>14a,16</sup> collectively they significantly reduce  
26 activation barriers *via* transition state stabilization.<sup>17,18</sup> Moreover, these conclusions were  
27 experimentally validated through ligand synthesis and subsequent kinetic analysis.<sup>14a</sup>  
28  
29  
30  
31  
32  
33  
34  
35  
36  
37  
38  
39  
40  
41  
42  
43  
44  
45  
46  
47  
48  
49  
50  
51  
52  
53  
54  
55  
56  
57  
58  
59  
60

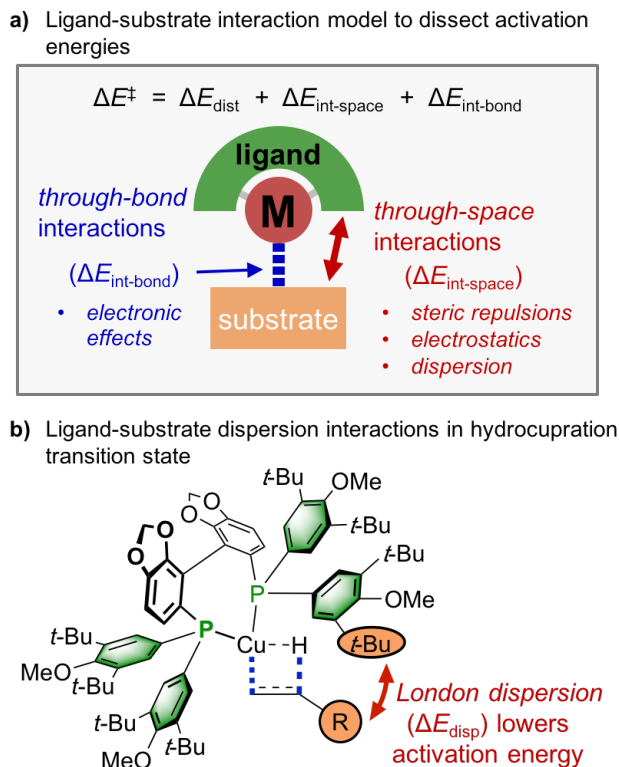
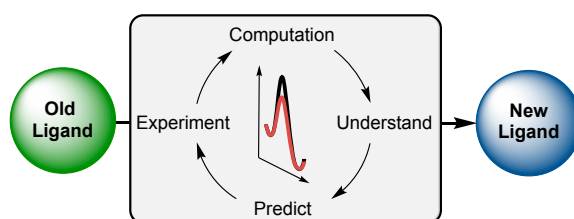


**Figure 2** a) Ligand-substrate interaction model to study the origin of reactivity in hydrocupration. b) London dispersion interactions lowering the hydrocupration barrier for **L2CuH**.

Building upon this knowledge, we undertook the challenge of designing a new family of ligands based on SEGPHOS **L1** to more efficiently facilitate the copper-hydride catalyzed *anti*-Markovnikov hydroamination reaction with terminal olefins. We theorized a more effective ligand system can be rationally designed by retaining the stabilizing dispersion effects of DTBM-SEGPHOS **L2** while incorporating other types of stabilizing through-bond and/or through-space interactions.<sup>19</sup> Specifically, we surmised that other types of weak non-covalent interactions with the olefin substrate,<sup>20</sup> may be harnessed by installation of hetero-atom-containing substituents on the *P*-aryl<sub>2</sub> groups. In addition, the through-bond stabilization between the CuH moiety and the substrate in the hydrocupration transition state can be fine-tuned by altering the electronic character of the ligands. However, when designing catalysts capable of

1  
2  
3 promoting reactivity through an assortment of stabilizing interactions, infinite possibilities are  
4 conceivable. With the unique ability to computationally quantify and experimentally verify these  
5 interactions, an iterative catalyst design approach was envisioned (Figure 3).<sup>21,22</sup> This approach  
6 comprised of four stages: (1) experimentally identify a suitable class of ligand derivatives; (2)  
7 using computational analysis to understand what key interactions can stabilize the transition  
8 state; (3) using this knowledge to computationally predict a more effective ligand and (4)  
9 experimentally test the ligand providing feedback for the next round of ligand optimization.



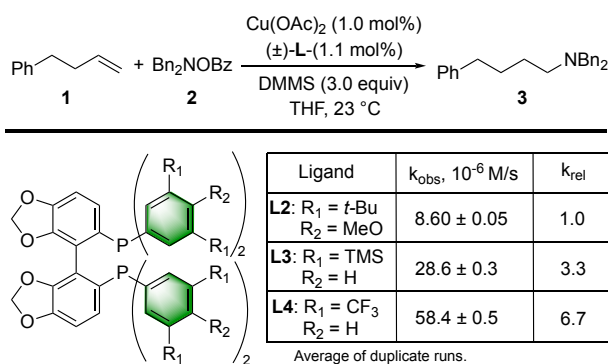
19  
20  
21  
22  
23  
24  
25  
26  
27 **Figure 3.** Project outline.

28  
29  
30  
31  
32 **3.1. Kinetic and computational analysis of SEGPHOS Ligands.** 3.1.1. *Preliminary*

33  
34 *Experimental Investigations with Symmetric SEGPHOS Ligands.* As described above, previous  
35 investigations indicated that primarily bulky substituents at the 3 and 5-positions on the *P*-aryl<sub>2</sub>  
36 groups were critical in facilitating the hydrocupration event with terminal olefins.<sup>14a</sup> This finding  
37 directed our preliminary studies to investigate SEGPHOS derivatives with substituents  
38 possessing different steric (TMS) and electronic (CF<sub>3</sub>) properties at these positions (Scheme 1).<sup>23</sup>  
39 To kinetically quantify and compare the effects of these ligands on the hydrocupration event 4-  
40 phenyl-1-butene (**1**) and *O*-benzoyl-*N,N*-dibenzylhydroxylamine (**2**) were selected as model  
41 substrates, because a first order dependence on the olefin had been shown previously for the  
42 hydroamination reaction with DTBM-SEGPHOS **L2**.<sup>24</sup> The initial rates were measured for the  
43 reaction with each ligand by monitoring the formation of hydroamination product **3** under typical  
44  
45  
46  
47  
48  
49  
50  
51  
52  
53  
54  
55  
56  
57  
58  
59  
60

copper hydride hydroamination conditions (1.0 mol% Cu(OAc)<sub>2</sub>, 1.1 mol% ligand, 0.36 M in THF, 23 °C) utilizing dimethoxymethylsilane (DMMS, 3.0 equiv/**1**) as the stoichiometric reductant. To allow for a straightforward comparison, the rate of hydroamination was measured first with DTBM-SEGPHOS **L2** ( $8.60 \pm 0.05$ )  $\times 10^{-6}$  M/s so that the rates could be normalized (Scheme 1).

**Scheme 1.** Initial kinetic analysis for symmetric ligands **L2**, **L3** and **L4**.



Following our standard protocol, the reaction employing TMS-SEGPHOS **L3** was found to be 3.3 times faster than that with DTBM-SEGPHOS **L2**, suggesting that the larger TMS substituents, with a Taft value of  $E_s' = 1.79$ , have stronger interactions with the olefin substrate than the *t*-Bu groups ( $E_s' = 1.49$ ) in DTBM-SEGPHOS **L2** (Scheme 1).<sup>25</sup> Interestingly, the hydroamination with the CF<sub>3</sub>-SEGPHOS **L4** derivative underwent the hydrocupration event 6.7 times faster than **L2** and 2.0 times faster than **L3** even though the CF<sub>3</sub> groups ( $E_s' = 0.78$ ) are smaller and presumably less polarizable.<sup>26</sup> This suggested that the fluorine-containing substituents have additional stabilizing effects that are stronger than simple London dispersion interactions as observed with **L2** and **L3**. The origin for this significant and unexpected rate increase for **L4** was revealed by computational investigations as detailed below.

1  
2  
3 *3.1.2. Computational Analysis of the Origin of Reactivity with Symmetric SEGPHOS*  
4 *Derivatives.* The preliminary experimental studies revealed promising results with the CF<sub>3</sub>-  
5 SEGPHOS **L4** derivative. However, it was unclear what further modifications could lead to  
6 additional reactivity enhancement.<sup>21,27</sup> Although successful predictions of new transition metal  
7 catalysts from computational results alone are still rare,<sup>28</sup> several examples have recently been  
8 described wherein a combination of computational and experimental evaluations has led to the  
9 discovery of catalysts with improved reactivity and selectivity.<sup>21,22</sup> Such synergetic efforts  
10 effectively utilize the predictive power of computation, while the experimental verification helps  
11 resolve the uncertainty of calculated energies and issues that cannot be readily addressed by  
12 computations alone, such as catalyst decomposition.<sup>29</sup>  
13  
14  
15  
16  
17  
18  
19  
20  
21  
22  
23  
24  
25  
26  
27  
28

29 *3.1.2.1 Computational Methods* Geometry optimizations and single-point energy calculations  
30 were carried out using Gaussian 09.<sup>30</sup> Geometries of intermediates and transition states were  
31 optimized using the B3LYP functional<sup>31</sup> with a mixed basis set of SDD for Cu and 6-31G(d) for  
32 other atoms in the gas phase. Vibrational frequency calculations were performed for all of the  
33 stationary points to confirm if each optimized structure is a local minimum or a transition state  
34 structure. Truhlar's quasi-harmonic corrections<sup>32</sup> were applied for entropy calculations using 100  
35 cm<sup>-1</sup> as the frequency cut-off. Solvation energy corrections were calculated in THF solvent with  
36 the CPCM continuum solvation model<sup>33</sup> based on the gas-phase optimized geometries. The  
37  $\omega$ B97X-D functional<sup>34</sup> with a mixed basis set of SDD for Cu and 6-311+G(d,p) for other atoms  
38 was used for solvation single-point energy calculations. The computed gas-phase activation  
39 energy ( $\Delta E^\ddagger$ ) was dissected using the following ligand-substrate interaction model analysis.<sup>35</sup>  
40  
41  
42  
43  
44  
45  
46  
47  
48  
49  
50  
51  
52  
53  
54  
55  
56  
57  
58  
59  
60

$$\Delta E^{\ddagger} = \Delta E_{\text{dist}} + \Delta E_{\text{int-bond}} + \Delta E_{\text{int-space}} \quad \text{eq. 1}$$

The distortion energy ( $\Delta E_{\text{dist}}$ )<sup>35</sup> is the sum of the energies required to distort the LCuH catalyst and the substrate into their transition state geometries.  $\Delta E_{\text{int-space}}$  was calculated from the interaction energy of a supramolecular complex of the phosphine ligand and the olefin substrate at the transition state geometry but in the absence of the CuH moiety ( $\Delta E_{\text{int-space}} = E_{\text{lig+sub}} - E_{\text{lig}} - E_{\text{sub}}$ ). Then, the through bond interaction was calculated from  $\Delta E_{\text{int-bond}} = \Delta E^{\ddagger} - \Delta E_{\text{dist}} - \Delta E_{\text{int-space}}$ . The  $\Delta E_{\text{dist}}$  and  $\Delta E_{\text{int-space}}$  were both calculated using the  $\omega$ B97X-D functional with the SDD basis set for Cu and 6-311+G(d,p) for other atoms. The  $\omega$ B97X-D functional was chosen because it has been shown to accurately describe non-covalent interactions,<sup>36</sup> which we expected to be important in this system. The computed free energy barriers using this method provided very good agreement with the experimental reaction rate constants (see SI for details and comparison with results from other functionals and solvation models). The through-space interaction energy ( $\Delta E_{\text{int-space}}$ ) between the ligand and the substrate is further dissected according to the following equation:

$$\Delta E_{\text{int-space}} = \Delta E_{\text{Pauli}} + \Delta E_{\text{elstat}} + \Delta E_{\text{pol}} + \Delta E_{\text{ct}} + \Delta E_{\text{disp}} \quad \text{eq. 2}$$

In accordance with our previous study, the dispersion energy component ( $\Delta E_{\text{disp}}$ ) was obtained from the difference of interaction energies calculated using MP2 and HF. The MP2 calculations were performed with Q-Chem 5.0 using the SOS(MI)-MP2 method in combination with the dual-basis set approach utilizing the db-cc-pVTZ basis set.<sup>37</sup> The  $\Delta E_{\text{Pauli}}$ ,  $\Delta E_{\text{elstat}}$ ,  $\Delta E_{\text{disp}}$ ,  $\Delta E_{\text{pol}}$ , and  $\Delta E_{\text{ct}}$  terms in eq 2 were calculated using the second-generation energy decomposition

1  
2  
3 analysis based on absolutely localized molecular orbitals<sup>38</sup> (ALMO-EDA) method implemented  
4 in Q-Chem 5.0.<sup>39</sup> The second generation ALMO-EDA provides further decomposition of the  
5 Pauli and electrostatic interaction ( $\Delta E_{\text{rep}}$ ) term into Pauli repulsion ( $\Delta E_{\text{Pauli}}$ ) and electrostatic  
6 ( $\Delta E_{\text{elstat}}$ ) energies, which is important in the analysis of through-space electrostatic interactions  
7 with the fluorinated ligands. To avoid double counting of dispersion, HF method with the 6-  
8 311G(d,p) basis set was employed in the energy decomposition analysis (EDA) calculations.  
9  
10  
11  
12  
13  
14  
15  
16  
17  
18

19 *3.1.2.2. Computational Analysis of Symmetric-SEGPHOS Ligands.* In order to fully understand  
20 the underlying principles and interactions that lead to the enhanced rate, an in-depth  
21 computational analysis was performed to study the origin of the different hydroamination  
22 reactivities between the DTBM-SEGPHOS **L2** and CF<sub>3</sub>-SEGPHOS **L4**-supported CuH catalysts.  
23  
24  
25  
26  
27

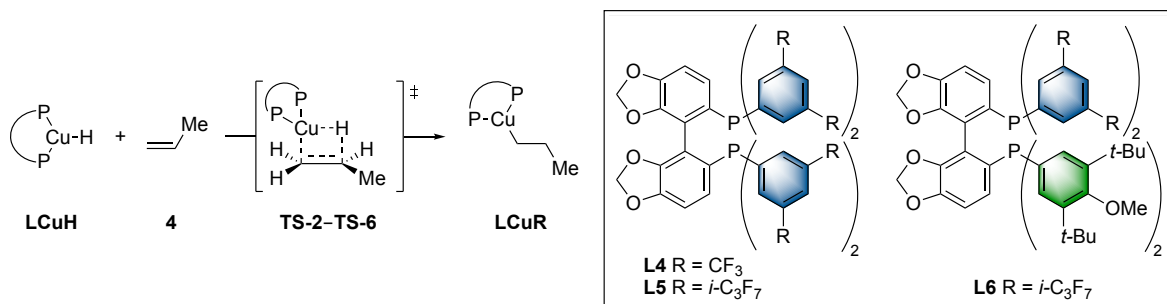
28 The activation energies of the rate-determining hydrocupration transition states were  
29 computed using propene (**4**) as the model substrate with the method outlined above (Table 1).  
30 The computed barrier of hydrocupration with the CF<sub>3</sub>-SEGPHOS **L4**CuH complex was in good  
31 agreement with the experimentally observed rate increase with **L4** compared to DTBM-  
32 SEGPHOS **L2**CuH ( $\Delta\Delta G_{\text{comp}}^{\ddagger} = 1.5$  kcal/mol vs  $\Delta\Delta G_{\text{exp}}^{\ddagger} = 1.1$  kcal/mol). In order to quantify  
33 the different factors that lead to the improved reactivity, the ligand-substrate interaction model  
34 analysis was employed to dissect the overall hydrocupration activation energies (Eqs. 1 and 2,  
35 see *Computational Methods* for details). Energy-decomposition analysis of the hydrocupration  
36 transition state with **L4**CuH revealed that the increase in the reaction rate was due to  
37 significantly stronger through-bond interactions ( $\Delta E_{\text{int-bond}}$ ) resulting in an extra 2.3 kcal/mol  
38 stabilization of **TS-4** compared to the DTBM-SEGPHOS-bound **TS-2**. This is because of the  
39 electron-withdrawing nature of the CF<sub>3</sub>-substituents which consequently results in enhanced  
40  
41  
42  
43  
44  
45  
46  
47  
48  
49  
50  
51  
52  
53  
54  
55  
56  
57  
58  
59  
60

1  
2  
3 Lewis acidity of the CuH catalyst and more favorable binding of the olefin substrate (see SI for  
4 details). While the through-space interaction energies ( $\Delta E_{\text{int-space}}$ ) are comparable in **TS-2** and  
5  
6 **TS-4**, the origins are different. Using the second-generation ALMO-EDA methods, the  $\Delta E_{\text{int-space}}$   
7  
8 term was further dissected into its individual energy components (Eq. 2). While **TS-2** is  
9  
10 stabilized by stronger attractive London dispersion ( $\Delta E_{\text{disp}} = -13.3$  kcal/mol for **TS-2** compared  
11  
12 to  $-10.7$  kcal/mol for **TS-4**), electrostatic interactions are more favorable in **TS-4** ( $\Delta E_{\text{elstat}} = 0.3$   
13  
14 kcal/mol for **TS-2** compared to  $-1.5$  kcal/mol for **TS-4**). The optimized geometry of **TS-4**  
15  
16 revealed multiple C–F $\cdots$ H–C contacts, which are responsible for the through-space electrostatic  
17  
18 interactions between **L4** and the olefin substrate thereby lowering  $\Delta E^\ddagger$  (Figure 4).  
19  
20  
21  
22  
23

24 Although the use of CF<sub>3</sub>-SEGPPOS **L4** leads to a relatively moderate increase of  
25  
26 reactivity, the computational analysis suggested types of modifications that might result in a  
27  
28 more effective ligand. Considering that the CF<sub>3</sub>-SEGPPOS **L4** ligated LCuH complex has  
29  
30 weakened dispersion interactions when compared to the **L2**CuH complex, we hypothesized that  
31  
32 the installation of a larger perfluorinated substituent would be beneficial. Since the *i*-C<sub>3</sub>F<sub>7</sub> group  
33  
34 is sterically more demanding than CF<sub>3</sub>, we assumed that it should increase stabilizing London  
35  
36 dispersion, while maintaining the favorable through-space electrostatic attractions and through-  
37  
38 bond electronic effects.  
39  
40  
41

42 Indeed, the calculated hydrocupration transition state **TS-5** indicated that the use of *i*-  
43  
44 C<sub>3</sub>F<sub>7</sub>-SEGPPOS **L5** as the ligand led to an additional 1.5 kcal/mol lower activation energy  
45  
46 compared to the hydrocupration with **L4**CuH (Table 1).  
47  
48  
49  
50  
51  
52  
53  
54  
55  
56  
57  
58  
59  
60

**Table 1.** Activation free energies of the hydrocupration transition states and energy components derived from the ligand-substrate interaction model.<sup>a</sup>



ligand	DTBM ( <b>L2</b> )	CF <sub>3</sub> ( <b>L4</b> )	<i>i</i> -C <sub>3</sub> F <sub>7</sub> ( <b>L5</b> )	DTBM- <i>i</i> -C <sub>3</sub> F <sub>7</sub> ( <b>L6</b> )
hydrocupration transition state	<b>TS-2</b>	<b>TS-4</b>	<b>TS-5</b>	<b>TS-6</b>
$\Delta G_{\text{solv}}^\ddagger$	20.2	18.7	17.2	17.0
$\Delta E^\ddagger$	-0.1	-1.0	-3.4	-3.0
distortion ( $\Delta E_{\text{dist}}$ )	28.6	29.5	28.8	27.9
through-bond interaction ( $\Delta E_{\text{int-bond}}$ )	-23.9	-26.2	-26.2	-25.4
through-space interaction ( $\Delta E_{\text{int-space}}$ )	-4.8	-4.3	-6.0	-5.6
Pauli repulsion ( $\Delta E_{\text{Pauli}}$ )	9.0	8.4	7.9	7.8
electrostatic ( $\Delta E_{\text{elstat}}$ )	0.3	-1.5	-1.2	-0.3
London dispersion ( $\Delta E_{\text{disp}}$ )	-13.3	-10.7	-11.9	-13.0
charge transfer ( $\Delta E_{\text{ct}}$ )	-0.2	-0.2	-0.1	0.0
polarization ( $\Delta E_{\text{pol}}$ )	-0.6	-0.4	-0.4	-0.4
$\Delta \Delta G_{\text{comp}}^\ddagger$	0.0	-1.5	-3.0	-3.2
$\Delta \Delta G_{\text{exp}}^\ddagger$	0.0	-1.1	-2.4	-2.4

<sup>a</sup> All energies are reported in kcal/mol. The activation energies ( $\Delta G_{\text{solv}}^\ddagger$  and  $\Delta E^\ddagger$ ) are with respect to the separated CuH catalyst and propene (**4**).  $\Delta \Delta G_{\text{comp}}^\ddagger$  values were calculated by subtracting  $\Delta G_{\text{solv}}^\ddagger$ -**L2** from  $\Delta G_{\text{solv}}^\ddagger$ -**LX**.  $\Delta \Delta G_{\text{exp}}^\ddagger$  were derived from the experimental relative rate constants ( $k_{\text{rel}}$ ).

The ligand-substrate interaction model analysis validated our hypothesis, as the  $\Delta E_{\text{dist}}$  and  $\Delta E_{\text{int-bond}}$  terms of **TS-5** remained largely unchanged when compared to **TS-4**. Meanwhile, the through-space interaction of **TS-5** was 1.7 kcal/mol more stabilizing. Further dissection of the

through-space interactions revealed that the primary reason for the increased reactivity was due to the increased London-dispersion interactions ( $\Delta E_{\text{disp}}$ ) in **TS-5**. To validate this computational prediction, we needed to experimentally measure the reactivity of *i*-C<sub>3</sub>F<sub>7</sub>-SEGPHOS-supported CuH catalyst **L5CuH**.

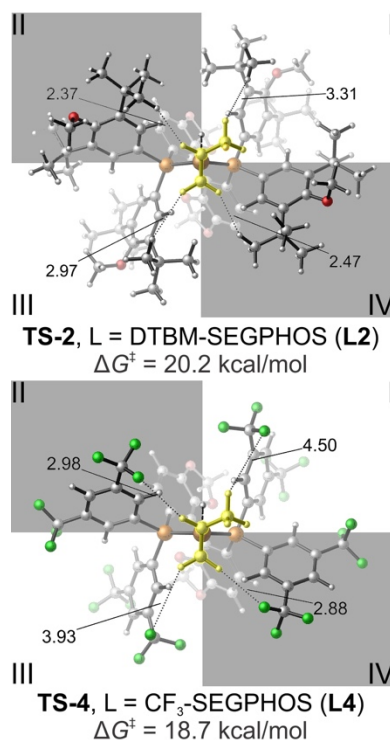
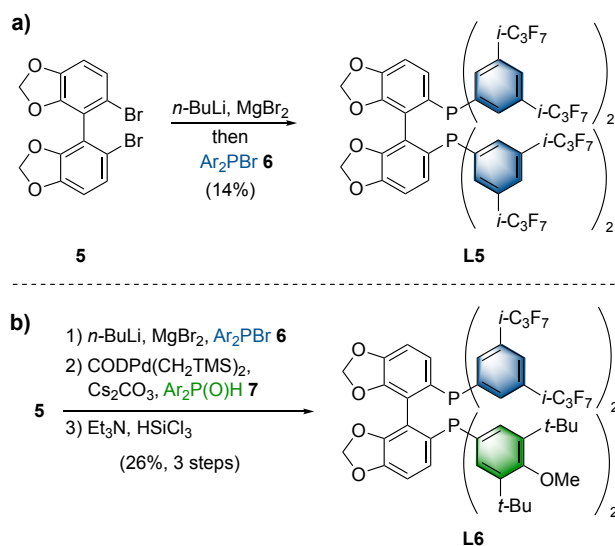


**Figure 4.** Optimized geometries of hydrocupration transition states with the DTBM-SEGPHOS (**TS-2**) and CF<sub>3</sub>-SEGPHOS ligands (**TS-4**). Distances are in Ångström [Å].

### 3.1.4. Synthesis and Kinetic Analysis of Hydroamination with the Symmetric *i*-C<sub>3</sub>F<sub>7</sub>-SEGPHOS

*Ligand.* Informed by the computational predictions described above, we set out to synthesize ligand **L5**. Adopting a closely related report by Yu, we were able to prepare **L5** from dibromide **5** and *bis*-(3,5-*i*-C<sub>3</sub>F<sub>7</sub>-C<sub>6</sub>H<sub>3</sub>)<sub>2</sub>PBr (**6**) in a single step (Scheme 2a).<sup>40</sup>

**Scheme 2.** Synthesis of SEGPHOS derivatives **L5** and **L6** (see Supporting Information for details).

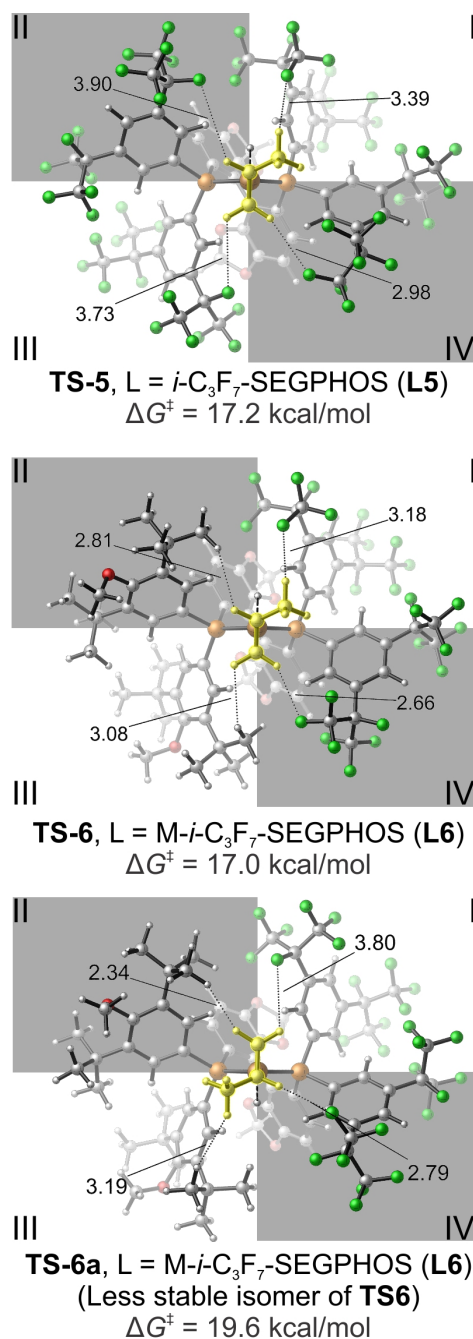


When **L5** was employed with the standard catalytic conditions, *vide supra*, the formation of hydroamination product **3** was observed to be 61 times faster than with **L2**, indicating that increased London dispersion interactions were indeed facilitating the hydrocupration event. However, only a short burst of reactivity was observed under the reaction conditions employing **L5**. This suggests that the **L5CuH** complex, although an active catalyst, was not stable under the reaction conditions (Figure 6, red curve).<sup>41</sup> This catalyst decomposition is most likely the consequence of the diminished Lewis basicity of the phosphorus atoms in **L5**, due to the electron-withdrawing nature of the *i*-C<sub>3</sub>F<sub>7</sub> substituents which results in weaker binding to the copper center. In order to exhibit both high reactivity and stability, the Lewis acidity of the copper center needed to be finely tuned.

**3.1.5. Hybrid-SEGPHOS Ligands** To harness the increased reactivity that we observed using the *i*-C<sub>3</sub>F<sub>7</sub> substituents without sacrificing the stability of the resulting complex, we had two options: either to synthesize and test various new derivatives with different substituents, in order to find a suitable ligand that provides a catalyst system that combines high activity and stability, or exchange one *P*-aryl<sub>2</sub> substituent for a more electron-donating group in order to stabilize the

1  
2  
3 resulting copper complex. To avoid significant structural changes at the 3- and 5-positions of the  
4 aryl groups, we reasoned that the merger of DTBM-L2 and *i*-C<sub>3</sub>F<sub>7</sub>-L5, the ligands with higher  
5 catalyst stability and reactivity, might result in the perfect balance of their respective beneficial  
6 interactions. This hypothesis found further support in examining the transition-state structure TS-  
7 5, in which the improved through-space ligand-substrate interactions primarily arise from the C-  
8 F···H-C interactions in the 1<sup>st</sup> and 4<sup>th</sup> quadrants (Figure 5). The *i*-C<sub>3</sub>F<sub>7</sub> groups in the 2<sup>nd</sup> and 3<sup>rd</sup>  
9 quadrants are further away from the substrate, and thus are less significant in promoting the  
10 hydrocupration step. Therefore, exchanging the *P*-aryl<sub>2</sub> groups in the 2<sup>nd</sup> and 3<sup>rd</sup> quadrants was  
11 not expected to significantly impact the enhanced reactivity gained from the *i*-C<sub>3</sub>F<sub>7</sub> moieties.  
12  
13  
14  
15  
16  
17  
18  
19  
20  
21  
22  
23  
24  
25

26 *3.1.5.1 Computational Studies of Hydrocupration with Hybrid-SEGPHOS Ligands* The  
27 computational investigations showed that the hydrocupration barrier for the hybrid SEGPHOS  
28 derivative L6CuH was similar to that of the symmetric derivative L5CuH (see Table 1). In the  
29 lowest energy transition state structure with L6 (TS-6, Figure 5), the methyl group on propene  
30 (4) prefers to be placed in the *i*-C<sub>3</sub>F<sub>7</sub>-occupied 1<sup>st</sup> quadrant, rather than the DTBM-occupied 3<sup>rd</sup>  
31 quadrant (TS-6a, Figure 5), indicating the C-F···H-C non-covalent interactions with the *i*-C<sub>3</sub>F<sub>7</sub>  
32 group are more favorable than the C-H···H-C interactions with the *t*-Bu group. Further energy  
33 decomposition analysis showed similar through-space interaction energies ( $\Delta E_{\text{int-space}}$ ) in TS-6  
34 and TS-5 (Table 1). While electrostatic interactions in TS-6 were slightly decreased relative to  
35 those in TS-5, London dispersion interactions were increased as a result of the larger *t*-butyl  
36 substituents in the 2<sup>nd</sup> and 3<sup>rd</sup> quadrants of TS-6. This finding indicated, that a comparable  
37 energy barrier of hydrocupration might be obtained from L6CuH.  
38  
39  
40  
41  
42  
43  
44  
45  
46  
47  
48  
49  
50  
51  
52  
53  
54  
55  
56  
57  
58  
59  
60



46 **Figure 5.** Optimized geometries of hydrocupration transition states with the *i*-C<sub>3</sub>F<sub>7</sub>-SEGPPOS  
47 (**TS-5**) and the hybrid DTBM-*i*-C<sub>3</sub>F<sub>7</sub>-SEGPPOS ligand (**TS-6** and **TS-6a**). Distances are  
48 reported in Ångström [Å].  
49

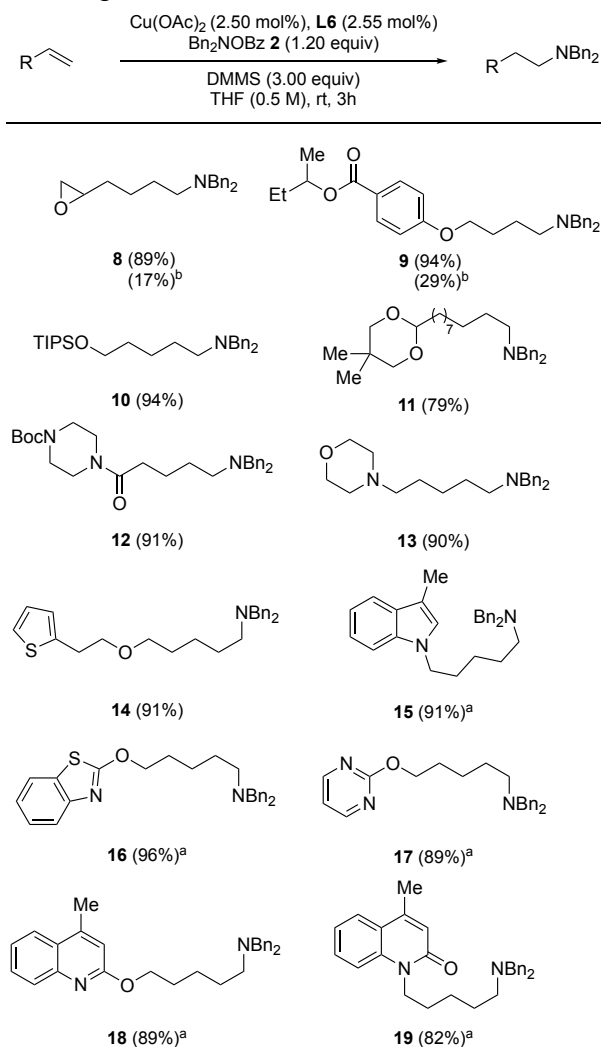
50  
51  
52 *3.1.5.2 Synthesis of Hybrid-SEGPPOS Ligands* To verify our hypothesis, a practical  
53  
54 synthetic sequence had to be developed to prepare this hybrid ligand. After extensive  
55  
56  
57  
58  
59  
60



1  
2  
3 **Figure 6.** Combined data for the formation of amination product **3** (see, supplemental material  
4 for details).  
5  
6  
7

8 *3.1.6. Demonstration of Hybrid-SEGPHOS Ligand L6 under Preparative Conditions.* In order  
9 for this newly developed ligand to be useful in a synthetic context, the observed rate increase  
10 would need to be maintained at preparatively relevant scales and on substrates bearing functional  
11 groups. After slight optimization of the reaction conditions, the scope of olefins was established  
12 using hydroxylamine ester **2** as the amine source (Table 2). The hydroamination of terminal  
13 olefins that contained various functional groups were surveyed at room temperature. Epoxide **8**,  
14 ester **9**, silyl ether **10**, and ketal **11** all provided the desired tertiary amine product in excellent  
15 yield. Moreover, substrates that contained a variety of heterocycles, such as piperazine **12**,  
16 morpholine **13**, and thiophene **14** also underwent smooth hydroamination at room temperature.  
17 Stronger Lewis bases found in heterocyclic compounds like indole **15**, benzothiazole **16**,  
18 pyrimidine **17**, and in quinolines **18** and **19** slightly inhibited the reaction, and thus their  
19 reactions required slightly elevated temperatures (40 °C) to reach full conversion within 3  
20 hours.<sup>43</sup> To compare our new catalyst to the current state-of-the-art catalyst, **L2**, epoxide **8** and  
21 ester **9** were subjected to these reaction conditions employing DTBM-**L2** as the ligand.<sup>4b</sup>  
22 Diminished yields of 17 and 29% were observed compared to 89 and 94% with **L6**, respectively.  
23 This demonstrates that the rate enhancement using this catalyst system is maintained under  
24 preparative reaction conditions.  
25  
26  
27  
28  
29  
30  
31  
32  
33  
34  
35  
36  
37  
38  
39  
40  
41  
42  
43  
44  
45  
46  
47  
48  
49  
50  
51  
52  
53  
54  
55  
56  
57  
58  
59  
60

**Scheme 3.** Isolated yields are reported as the average of two runs. Standard reaction conditions: terminal olefin (0.50 mmol),  $\text{Bn}_2\text{NOBz}$  (**2**) (0.60 mmol),  $\text{Cu}(\text{OAc})_2$  (2.50 mol%), **L6** (2.55 mol%), DMMS (1.50 mmol), THF (1.0 mL), 23 °C, 3h. <sup>a</sup>40 °C. <sup>b</sup> DTBM-SEGPHOS was used in place of **L6** and NMR yields are provided.



## CONCLUSION

This study demonstrates how the combination of mechanistic insights, computational prediction, and experimental verification can successfully benefit ligand development. Using this synergistic approach we were able to discover a new hybrid ligand **L6** that is capable of promoting the *anti*-Markovnikov hydroamination of unactivated, terminal olefins with a 62 fold

1  
2  
3 rate increase compared to DTBM-SEGPHOS **L2**. By employing energy decomposition analysis  
4  
5 methods, we were able to deconvolute each individual energy contributions of the steric,  
6  
7 electronic, and dispersion effects that comprise the hydrocupration barrier. During the course of  
8  
9 our investigation we identified that in addition to London dispersion, both electrostatic C–F···H–  
10  
11 C non-covalent interactions and inductive effects of the *i*-C<sub>3</sub>F<sub>7</sub> substituents are capable of  
12  
13 lowering the energy barrier for hydrocupration even further. Ultimately, the merger of both  
14  
15 DTBM and *i*-C<sub>3</sub>F<sub>7</sub> substituents was key to success in designing **L6** with balanced stability and  
16  
17 reactivity. Furthermore, a modular and robust synthetic sequence to access these novel hybrid  
18  
19 ligand structures was devised, that allowed for its gram-scale synthesis. In addition, the  
20  
21 effectiveness of the catalyst system employing **L6** was proven under preparative conditions. We  
22  
23 anticipate that this rational ligand design approach can be utilized in other catalytic systems  
24  
25 providing accelerated reaction development.  
26  
27  
28  
29

## 30 SUPPORTING INFORMATION

31  
32  
33 The Supporting Information is available free of charge on the [ACS Publications website](#)  
34  
35 at DOI: [XX](#). Full computational and experimental procedures along with characterization  
36  
37 data and copies of <sup>1</sup>H, <sup>13</sup>C, <sup>31</sup>P, and <sup>19</sup>F, spectra, along with full kinetic data are provided.  
38  
39  
40

## 41 AUTHOR INFORMATION

42 Corresponding Authors

43 [sbuchwal@mit.edu](mailto:sbuchwal@mit.edu)

44 [pengliu@pitt.edu](mailto:pengliu@pitt.edu)

45  
46  
47  
48  
49 Author Contributions

50  
51 †A.A.T., K.S. and I.K. contributed equally to this work.  
52  
53  
54  
55  
56  
57  
58  
59  
60

## ACKNOWLEDGMENT

This material is based upon work supported by the NIH Postdoctoral Fellowship Program under Grant No. 1F32GM125163 (A.A.T.), Leopoldina - National Academy of Science under Grant No. LPDS2017-08 (K.S.) and the NIH (Grant No. GM122483 and R35GM128779). Any opinions, findings, conclusions, or recommendations expressed in this material are those of the authors and do not necessarily reflect the views of the NIH. We are grateful to Drs. Peter Müller and Charlene Tsay for crystallographic analysis, and we acknowledge Richard Liu and Drs. Christine Nguyen and Scott McCann for assistance in the preparation of this manuscript. Calculations were performed at the Center for Research Computing at the University of Pittsburgh and the Extreme Science and Engineering Discovery Environment (XSEDE) supported by the NSF.

## REFERENCES

- (1) Zhu, S.; Niljianskul, N.; Buchwald, S.L. *J. Am. Chem. Soc.* **2013**, *135*, 15746–15749.
- (2) Miki, Y.; Hirano, K.; Satoh, T.; Miura, M. *Angew. Chem. Int. Ed.* **2013**, *52*, 10830–10834.
- (3) (a) Pirnot, M.T.; Wang, Y.M.; Buchwald, S.L. *Angew. Chem. Int. Ed.* **2016**, *55*, 48–57. (b) Zhu, S.; Buchwald, S.L. *J. Am. Chem. Soc.* **2014**, *136*, 15913–15916.
- (4) Niljianskul, N.; Zhu, S.; Buchwald, S.L. *Angew. Chem. Int. Ed.* **2015**, *54*, 1638–1641.
- (5) (a) Shi, S.L.; Buchwald, S.L. *Nat Chem.* **2015**, *7*, 38–44. (b) Severin, R.; Doye, S. *Chem. Soc. Rev.* **2007**, *36*, 1407–1420.
- (6) (a) Friis, S.D.; Pirnot, M.T.; Dupuis, L.N.; Buchwald, S.L. *Angew. Chem. Int.* **2017**, *56*, 7242–7246. (b) Yang, Y.; Shi, S.L.; Niu, D.; Liu, P.; Buchwald, S.L. *Science.* **2015**, *349*, 62–66.
- (7) For representative examples of other methods of hydroamination, see: (a) Musacchio, A.J.; Lainhart, B.C.; Zhang, X.; Naguib, S.G.; Sherwood, T.C.; Knowles, R.R. *Science.* **2017**, *355*, 727–750. (b) Ensign, S.C.; Venable, E.P.; Kortman, G.D.; Weir, L.J.; Hull, K.L. *J. Am. Chem. Soc.* **2015**, *137*, 13748–13751. (c) Nguyen, T.M.; Manohar, N.;

- 1  
2  
3  
4  
5  
6  
7  
8  
9  
10  
11  
12  
13  
14  
15  
16  
17  
18  
19  
20  
21  
22  
23  
24  
25  
26  
27  
28  
29  
30  
31  
32  
33  
34  
35  
36  
37  
38  
39  
40  
41  
42  
43  
44  
45  
46  
47  
48  
49  
50  
51  
52  
53  
54  
55  
56  
57  
58  
59  
60
- 
- Nicewicz, D.A.; *Angew. Chem. Int.* **2014**, *53*, 6198–6201. (d) Banerjee, D.; Junge, K.; Beller, M. *Org. Chem. Front.* **2014**, *1*, 368–372. (e) Rucker, R.P.; Whittaker, A.M.; Dang, H.; Lalic, G. *J. Am. Chem. Soc.* **2012**, *134*, 6571–6574. (f) Shapiro, N.D.; Rauniyar, V.; Hamilton, G.L.; Wu, J.; Toste, D. *Nature*, **2011**, *470*, 245–249. (g) Seayad, J.; Tillack, A.; Hartung, C.G.; Beller, M. *Adv. Synth. Catal.* **2002**, *344*, 795–813. (h) Schlummer, B.; Hartwig, J.F. *Org. Lett.* **2002**, 1471–1474.
- (8) (a) Bernoud, E.; Lepori, C.; Mellah, M.; Schulz, E.; Hannedouche, J. *Catal. Sci. Technol.* **2015**, *5*, 2017–2037. (b) Hultsch, K.C. *Org. Biomol. Chem.* **2005**, *3*, 1819–1824.
- (9) Dewick, P. M. *Medicinal natural products: a biosynthetic approach*, 3<sup>rd</sup> edition. ed., Wiley, Chichester, West Sussex, England; New York, NY, USA, 2009.
- (10) For reviews of methods for the synthesis of amines, see: (a) Baxter, E.W.; Reitz, A.B. *Organic Reactions* **2002**, *59*, 1–741. (b) *Chiral Amine Synthesis*; Nugent, T. C., Ed.; Wiley-VCH: Weinheim, 2010.
- (11) Liu, R. Y.; Buchwald, S. L. *Org. Synth.* **2018**, *95*, 80–96.
- (12) Bandar, J.S.; Pirnot, M.T.; Buchwald, S.L. *J. Am. Chem. Soc.* **2015**, *137*, 14812–14818.
- (13) For representative examples of aminoboration, see: Xi, Y.; Hartwig, J.F. *J. Am. Chem. Soc.* **2017**, *139*, 12758–12772. (b) Lee, J.; Radomkit, S.; Torker, S.; Pozo, J.D.; Hoveyda, A.H. *Nat. Chem.* **2017**, *10*, 99–108.
- (14) (a) Lu, G.; Liu, R.Y.; Yang, Y.; Fang, C.; Lambrecht, D.S.; Buchwald, S.L.; Liu, P. *J. Am. Chem. Soc.* **2017**, *139*, 16548–16555. (b) Tobisch, S. *Chem. Sci.* **2017**, *8*, 4410–4423.
- (15) We propose a mechanism that is consistent with all of the current data but we cannot exclude the possibility that the C-N bond forming step occurs through an outersphere process.
- (16) Echeverria, J.; Aullon, G.; Danovich, D.; Shaik, S.; Alvarez, S. *Nature Chem.*, **2011**, *3*, 323–330.
- (17) (a) Neel, A.J.; Hilton, M.J.; Sigman, M.S.; Toste, F.D. *Nature* **2017**, *543*, 637–646. (b) Wagner, J. P.; Schreiner, P. R. *Angew. Chem., Int. Ed.* **2015**, *54*, 12274–12296.
- (18) (a) Xu, X.; Liu, P.; Lesser, A.; Sirois, L. E.; Wender, P. A.; Houk, K. N. *J. Am. Chem. Soc.* **2012**, *134*, 11012–11025. (b) Wolters, L. P.; Koekkoek, R.; Bickelhaupt, F. M. *ACS Catal.* **2015**, *5*, 5766–5775. (c) Lyngvi, E.; Sanhueza, I. A.; Schoenebeck, F. *Organometallics* **2015**, *34*, 805–812. (d) Meyer, T. H.; Liu, W.; Feldt, M.; Wuttke, A.; Mata, R. A.; Ackermann, L. *Chem. - Eur. J.* **2017**, *23*, 5443–5447. (e) Cundari, T. R.; Jacobs, B. P.; MacMillan, S. N.; Wolczanski, P. T. *Dalton Trans.*, **2018**, *47*, 6025–6030.

- 1  
2  
3  
4  
5  
6 (19) (a) Hale, L.V.A.; Szymczak, N.K. *ACS Catal.* **2018**, *8*, 6446–6461. (b) Chattopadhyay,  
7 B.; Dannatt, J.E.; Sanctis, I.L.A.D.; Gore, K.A.; Maleczka, R.E.; Singleton, D.A.; Smith,  
8 M.R. *J. Am. Chem. Soc.* **2017**, *139*, 7864–7871. (c) Davis, H.J.; Mihai, M.T.; Phipps,  
9 R.J. *J. Am. Chem. Soc.* **2016**, *138*, 12759–12762 (d) Kuninobu, Y.; Ida, H.; Nishi, M.;  
10 Kanai, M. *Nat. Chem.* **2015**, *7*, 712–717.  
11  
12 (20) (a) Kui, S. C. F.; Zhu, N.; Chan, M. C. W. *Angew. Chem. Int. Ed.* **2003**, *42*, 1628–1632.  
13 (b) Mitani, M.; Mohri, J.; Yoshida, Y.; Saito, J.; Ishii, S.; Tsuru, K.; Matsui, S.;  
14 Furuyama, R.; Nakano, T.; Tanaka, H.; Kojoh, S.; Matsugi, T.; Kashiwa, N.; Fujia, T. J.  
15 *Am. Chem. Soc.*, **2002**, *124*, 13, 3327–3336.  
16  
17 (21) (a) Luo, S.X.; Engle, K.M.; Dong, X.; Heji, A.; Takase, M.K.; Henling, L.M.; Liu, P.;  
18 Houk, K.N.; Grubbs, R.H. *ACS Catal.* **2018**, *8*, 4600–4611. (b) Burrows, L.C.;  
19 Jesikiewicz, L.T.; Lu, G.; Geib, S.J.; Liu, P.; Brummond, K.M. *J. Am. Chem. Soc.* **2017**,  
20 *139*, 15022–15032.  
21  
22 (22) (a) Straker, R. N.; Mekareeya, A.; Paton, R. S.; Anderson, E. A. *Nat. Commun.* **2016**, *7*,  
23 10109–10118. (b) Kwon, D.; Fuller, J. T.; Kilgore, U. J.; Sydora, O. L.; Bischof, S. M.;  
24 Ess, D. H. *ACS Catal.*, **2018**, *8*, 1138–1142. (c) Nielsen, M. C.; Bonney, K. J.;  
25 Schoenebeck, F. *Angew. Chem. Int. Ed.* **2014**, *53*, 5903–5906. (d) Bernales, V.; League,  
26 A. B.; Li, Z.; Schweitzer, N. M.; Peters, A. W.; Carlson, R. K.; Hupp, J. T.; Cramer, C.  
27 J.; Farha, O. K.; Gagliardi, L. *J. Phys. Chem. C* **2016**, *120*, 23576–23583. (e) Sinha, I.;  
28 Lee, Y.; Bae, C.; Tussupbayev, S.; Lee, Y.; Seo, M.; Kim, J.; Baik, M.; Lee, Y.; Kim, H.  
29 *Catal. Sci. Technol.*, **2017**, *7*, 4375–4387. (f) Wang, Y.; Wang, J.; Su, J.; Huang, F.; Jiao,  
30 L.; Liang, Y.; Yang, D.; Zhang, S.; Wender, P. A.; Yu, Z.-X. *J. Am. Chem. Soc.* **2007**,  
31 *129*, 10060–10061. (g) Occhipinti, G.; Koudriavtsev, V.; Tönnroos, K. W.; Jensen, V. R.  
32 *Dalton Trans.* **2014**, *43*, 11106–11117.  
33  
34 (23) Ligands **L2** and **L3** were prepared according to: Sevov, C.S.; Hartwig, J.F. *J. Am. Chem.*  
35 *Soc.*, **2014**, *136*, 10625–10631.  
36  
37 (24) The hydrocupration event has been shown previously to be the rate determining step for  
38 terminal olefins with DTBM-SEGPHOS, see ref 13. Additionally, ligand **L6** exhibited  
39 clean first order profiles along with a first order dependence on the olefin substrate, see  
40 supplementary material.  
41  
42 (25) Macphee, J.A.; Panaye, A.; Dubois, J.E. *Tetrahedron*, **1978**, *34*, 2253–3562.  
43  
44 (26) O’Hagan, D. *Chem. Soc. Rev.* **2008**, *37*, 308–319.  
45  
46 (27) Iwamoto, H.; Imamoto, T.; Ito, H. *Nat. Commun.* **2018**, *9*, 2290.  
47  
48 (28) (a) Guan, Y.; Wheeler, S. E. *Angew. Chem. Int. Ed.* **2017**, *56*, 9101–9105. (b) Poree, C.;  
49 Schoenebeck, F. *Acc. Chem. Res.*, **2017**, *50*, 605–608.  
50  
51  
52  
53  
54  
55  
56  
57  
58  
59  
60

- (29) Sperger, T.; Sanhueza, I. A.; Schoenebeck, F. *Acc. Chem. Res.*, **2016**, *49*, 1311–1319.
- (30) Frisch, M. J.; Trucks, G. W.; Schlegel, H. B.; Scuseria, G. E.; Robb, M. A.; Cheeseman, J. R.; Scalmani, G.; Barone, V.; Mennucci, B.; Petersson, G. A.; Nakatsuji, H.; Caricato, M.; Li, X.; Hratchian, H. P.; Izmaylov, A. F.; Bloino, J.; Zheng, G.; Sonnenberg, J. L.; Hada, M.; Ehara, M.; Toyota, K.; Fukuda, R.; Hasegawa, J.; Ishida, M.; Nakajima, T.; Honda, Y.; Kitao, O.; Nakai, H.; Vreven, T.; Montgomery, J. A., Jr.; Peralta, J. E.; Ogliaro, F.; Bearpark, M.; Heyd, J. J.; Brothers, E.; Kudin, K. N.; Staroverov, V. N.; Kobayashi, R.; Normand, J.; Raghavachari, K.; Rendell, A.; Burant, J. C.; Iyengar, S. S.; Tomasi, J.; Cossi, M.; Rega, N.; Millam, N. J.; Klene, M.; Knox, J. E.; Cross, J. B.; Bakken, V.; Adamo, C.; Jaramillo, J.; Gomperts, R.; Stratmann, R. E.; Yazyev, O.; Austin, A. J.; Cammi, R.; Pomelli, C.; Ochterski, J. W.; Martin, R. L.; Morokuma, K.; Zakrzewski, V. G.; Voth, G. A.; Salvador, P.; Dannenberg, J. J.; Dapprich, S.; Daniels, A. D.; Farkas, Ö.; Foresman, J. B.; Ortiz, J. V.; Cioslowski, J.; Fox, D. J. *Gaussian 09*, Revision D.01; Gaussian, Inc.: Wallingford, CT, 2009.
- (31) (a) Lee, C.; Yang, W.; Parr, R. G. *Phys. Rev. B* **1988**, *37*, 785; (b) Becke, A. D. *J. Chem. Phys.* **1993**, *98*, 5648–5652.
- (32) Ribeiro, R. F.; Marenich, A. V.; Cramer, C. J.; Truhlar, D. G. *J. Phys. Chem. B* **2011**, *115*, 14556–14562.
- (33) (a) Cossi, M.; Rega, N.; Scalmani, G.; Barone, V. *J. Comp. Chem.*, **2003**, *24*, 669–681. (b) Barone, V.; Cossi, M. *J. Phys. Chem. A*, **1998**, *102*, 1995–2001.
- (34) Chai, J. D.; Head-Gordon, M. *Phys. Chem. Chem. Phys.*, **2008**, *10*, 6615–6620.
- (35) Bickelhaupt, F. M.; Houk, K. N. *Angew. Chem., Int. Ed.* **2017**, *56*, 10070–10086.
- (36) (a) Peverati, R.; Truhlar, D. G. *J. Phys. Chem. Lett.*, **2011**, *21*, 2810–2817. (b) Burns, L. A.; Vázquez-Mayagoitia, A.; Sumpter, B. G.; Sherrill, C. D. *J. Chem. Phys.* **2011**, *134*, 084107.
- (37) (a) Distasio, R. A., Jr; Head-Gordon, M. *Mol. Phys.* **2007**, *105*, 1073–1083. (b) Steele, R. P.; DiStasio, R. A.; Shao, Y.; Kong, J.; Head-Gordon, M. *J. Chem. Phys.* **2006**, *125*, 074108.
- (38) (a) Horn, P. R.; Head-Gordon, M. *J. Chem. Phys.* **2016**, *144*, 084118. (b) Horn, P. R.; Mao, Y.; Head-Gordon, M. *J. Chem. Phys.* **2016**, *144*, 114107. (c) Horn, P. R.; Mao, Y.; Head-Gordon, M. *Phys. Chem. Chem. Phys.*, **2016**, *18*, 23067–23079.
- (39) Shao, Y.; Gan, Z.; Epifanovsky, E.; Gilbert, A. T. B.; Wormit, M.; Kussmann, J.; Lange, A. W.; Behn, A.; Deng, J.; Feng, X.; Ghosh, D.; Goldey, M.; Horn, P. R.; Jacobson, L. D.; Kaliman, I.; Khaliullin, R. Z.; Kus, T.; Landau, A.; Liu, J.; Proynov, E. I.; Rhee, Y.

M.; Richard, R. M.; Rohrdanz, M. A.; Steele, R. P.; Sundstrom, E. J.; Woodcock, H. L.; Zimmerman, P. M.; Zuev, D.; Albrecht, B.; Alguire, E.; Austin, B.; Beran, G. J. O.; Bernard, Y. A.; Berquist, E.; Brandhorst, K.; Bravaya, K. B.; Brown, S. T.; Casanova, D.; Chang, C.-M.; Chen, Y.; Chien, S. H.; Closser, K. D.; Crittenden, D. L.; Diedenhofen, M.; DiStasio, R. A.; Do, H.; Dutoi, A. D.; Edgar, R. G.; Fatehi, S.; Fusti-Molnar, L.; Ghysels, A.; Golubeva-Zadorozhnaya, A.; Gomes, J.; Hanson-Heine, M. W. D.; Harbach, P. H. P.; Hauser, A. W.; Hohenstein, E. G.; Holden, Z. C.; Jagau, T.-C.; Ji, H.; Kaduk, B.; Khistyayev, K.; Kim, J.; Kim, J.; King, R. A.; Klunzinger, P.; Kosenkov, D.; Kowalczyk, T.; Krauter, C. M.; Lao, K. U.; Laurent, A. D.; Lawler, K. V.; Levchenko, S. V.; Lin, C. Y.; Liu, F.; Livshits, E.; Lochan, R. C.; Luenser, A.; Manohar, P.; Manzer, S. F.; Mao, S.-P.; Mardirossian, N.; Marenich, A. V.; Maurer, S. A.; Mayhall, N. J.; Neuscamman, E.; Oana, C. M.; Olivares-Amaya, R.; O'Neill, D. P.; Parkhill, J. A.; Perrine, T. M.; Peverati, R.; Prociuk, A.; Rehn, D. R.; Rosta, E.; Russ, N. J.; Sharada, S. M.; Sharma, S.; Small, D. W.; Sodt, *A. Mol. Phys.* **2015**, 113, 184–215

- (40) The corresponding diarylchlorophosphine resulted in no product formation; see: Liu, L.; Wu, H.C.; Yu, J.Q.; *Chem. Eur. J.* **2011**, 17, 10828–10831.
- (41) Colloidal copper was observed after a few minutes along with the observation of unbound **L5**.
- (42) The structure of **L6** was additionally validated by single crystal X-ray analysis (see supplementary information for details).
- (43) The reactions of substrates incorporating an imidazole unit resulted in no product formation, presumably due to the imidazole's Lewis basicity.

